DOI: 10.1002/ ()

Article type:

Anchoring Charge Selective Self-Assembled Monolayers for Tin–Lead Perovskite Solar Cells

*Zuhong Zhang, Rui Zhu, Ying Tang, Zhenhuang Su, Shuaifeng Hu, Xu Zhang, Junhan Zhang, Jinbo Zhao, Yunchang Xue, Xingyu Gao, Guixiang Li, Jorge Pascual, Antonio Abate, Meng Li**

Z. Zhang, Dr. R. Zhu, Y. Tang, X. Zhang, J. Zhao, Y. Xue, Prof. Dr. M. Li
Key Lab for Special Functional Materials of Ministry of Education, National & Local Joint Engineering Research Center for High-efficiency Display and Lighting Technology, School of Materials Science and Engineering, and Collaborative Innovation Center of Nano Functional Materials and Applications, Henan University
Kaifeng 475004, P. R. China
E-mail: mengli@henu.edu.cn

Dr. Z. Su, J. Zhang, Prof. Dr. X. Gao
Shanghai Synchrotron Radiation Facility (SSRF)
Shanghai Advanced Research Institute
Chinese Academy of Sciences
239 Zhangheng Road, Shanghai 201204, P. R. China

Dr. S. Hu
Clarendon Laboratory
Department of Physics
University of Oxford
Parks Road, Oxford, OX1 3PU

Dr. J. Pascual
POLYMAT, University of the Basque Country UPV/EHU
Centro Joxe Mari Korta Center
Tolosa Avenue, 72, 20018 Donostia-San Sebastián, Spain

Dr. G. Li
Institute of Chemical Sciences and Engineering
École Polytechnique Fédérale de Lausanne (EPFL)
CH-1015 Lausanne, Switzerland

Dr. G. Li, Prof. Dr. A. Abate
Helmholtz-Zentrum Berlin für Materialien und Energie GmbH
Hahn-Meitner-Platz 1, 14109 Berlin, Germany

Abstract: Self-assembled monolayers (SAMs) have displayed great potential for improving efficiency and stability in p-i-n perovskite solar cells. The anchoring of SAMs at the conduction metal oxide substrates and its interaction with perovskite materials must be rationally tailored to ensure efficient charge carrier extraction and improved quality of the perovskite films. Herein, we selected SAM molecules with different anchor groups and alkyl chain lengths to control interaction with perovskite in the p-i-n mixed Sn–Pb perovskite solar cells. We found that the carboxylate group exhibits appropriate interaction and is more favourable for orientation and arrangement monolayer than that of the phosphate group, which is beneficial for interaction between SAMs and perovskite. This results in reduced non-radiative recombination and enhanced crystallinity. In addition, the short chain length also led to an improved energy level alignment of SAMs with perovskite, improving hole extraction. As a result, the narrow bandgap (~1.25 eV) Sn–Pb perovskite solar cell devices showed efficiencies of up to 23.1% with an open circuit voltage of up to 0.89 V. Unencapsulated devices retained 93% of their initial efficiency after storage in N_2 atmosphere for over 2500 hours. Overall, this work highlights the underexplored potential of SAMs for perovskite photovoltaics and provides essential findings on the influence of their structural modification.
Keywords: Sn-Pb perovskite; SAMs; Interface engineering; Anchoring group; Charge carrier dynamics

1. Introduction

Metal-halide perovskite solar cells (PSCs) have achieved power conversion efficiency (PCE) values of over 26% with the single junction device configuration.[1] The low-cost solution[2-4] and vacuum-base[5, 6] fabrication protocols suggest the promising commercial potential of this technology.

Nowadays, leading-efficiency single-junction PSCs are prepared based on a light-absorbing layer prepared by neat Pb perovskite materials with a bandgap of 1.5-1.6 eV[7, 8]. According to the Shockley–Queisser limit, the most suitable bandgap for generating the highest achievable PCE of single junction solar cells is 1.2-1.4 eV[9]. In this sense, narrow bandgap (~1.25 eV) mixed tin–lead (Sn–Pb) perovskites are one of the main candidates to attain the highest PCE, with current records approaching 24%[10-13], thanks to the anomalous band gap behaviour [14, 15]. In addition, this exceptionally narrow bandgap perovskite material also shows successful application in the all-perovskite double[16] and multi-junction tandem photovoltaics as the rear sub-absorber[17-19], which reduces the thermalisation losses and increases the PCE of the devices[11, 20], with the record of up to 29.1%[21]. However, the range of substrates in which these materials can be successfully processed is limited, with poly(3,4-ethylenedioxythiophene)-poly(styrenesulfonate) (PEDOT: PSS) as the most widely employed platform. The acidic and hygroscopic nature of PEDOT: PSS, however, detrimentally affects the long-term stability of the perovskite materials, hindering the further advancement of the Sn–Pb perovskite-based photovoltaic technology.

In this regard, self-assembling materials have recently shown excellent performance in p-i-n PSCs as bottom interface modifiers[8, 22, 23]. These materials can anchor at the surface of metallic oxide to assemble dense and ordered monolayers, regulating the work function (WF), and enhancing the blocking of electrons and extraction of holes from the perovskite film to the electrode[24-26]. Compared with traditional hole transport layers[27], self-assembled monolayers (SAMs) show better feasibility in tuning their energy levels to improve the alignment with perovskite[22, 26, 28, 29] and no necessity of the laborious electronic doping[27, 30, 31]. For example, varying the functional groups of SAMs allows adjusting the charge extraction ability by modulating the dipole moment and further altering WF[22, 26, 28, 32].

SAMs based on carbazole show suitable alignment to the valence band maximum (VBM) of the perovskite and a significantly reduced nonradiative recombination, resulting in faster charge extraction[33, 34]. Anchor groups and alkyl chain lengths also were indicated to affect charge transfer rates and electron trapping[22, 32, 35]. Nevertheless, the nature of the interaction of SAMs based on different anchor groups and alkyl chain lengths with perovskite is a less-explored aspect, which could passivate buried interface defects to affect charge carrier dynamics and

stability[29, 36-38]. Meanwhile, the buried interface also affects perovskite crystallization, which determines the quality of final films[32, 37, 39, 40].

In this work, we present diverse structurally modified SAMs for mixed Sn–Pb PSCs with enhanced efficiency and stability. We investigated how anchor groups and alkyl chain length influence charge carrier dynamics at the buried interface and the quality of the perovskite films. Here, we selected three SAMs, i.e., 2-(9H-carbazol-9-yl)ethyl]phosphonic acid (2PACz), 3-(9-carbazolyl)propionic acid (9CPA), and (9-carbazolyl)acetic acid (9CAA), in which 9CPA and 9CAA display superior interaction with Sn–Pb perovskite at the interface, due to a reduction in the deviation angles between these two SAMs and Sn–Pb perovskite concerning that of 2PACz. The favourable contacts enhance perovskite crystallinity and suppress interface non-radiative recombination as suggested by grazing-incidence wide-angle X-ray scattering (GIWAXS) and transient photocurrent (TPC) measurements, respectively. With the ultraviolet photoelectron spectroscopy (UPS) measurement results, we found that the energy level alignment between 9CAA and Sn–Pb perovskite is favourable for charge carrier extraction. Finally, we obtained a PCE of 23.1% for the champion device fabricated with 9CAA, and the devices presented considerably improved stability, retaining 93% of their initial efficiency after 2500 h stored in a nitrogen-filled glovebox.

2. Result and Discussion

2.1 Interface mechanism of different SAMs

The SAMs were explored based on the p-i-n device structure of fluorine-doped tin oxide (FTO)/SAMs/$Cs_{0.1}FA_{0.6}MA_{0.3}Pb_{0.5}Sn_{0.5}I_3$/fullerene ($C_{60}$)/2,9-dimethyl-4,7-diphenyl-1,10-phenanthroline (BCP)/silver (Ag) (**Figure 1a**). In particular, the SAMs that we studied were 2PACz, 9CPA, and 9CAA. The interaction between SAMs and the metal oxide contact FTO was confirmed by X-ray photoelectron spectroscopy (XPS) (**Figure 1b**). To obtain the interface properties at the atomic and molecular level, we used first-principles calculations. As shown in **Figure 1c-e and S1**, the orientation and arrangement of the organic monolayers below Sn-Pb perovskite are dominated by the SAMs molecules' self-assembly. The length of carbazole in SAMs and the diagonal length of Sn-Pb-based perovskite are 8.95 Å and 8.81 Å, respectively. The different lengths result in a deviation angle between SAM molecules and Sn-Pb perovskite. The longer SAMs deviate from the perovskite diagonal when docking. As a result, the deviation angles of the 2PACz and two iodine ions in Sn-Pb perovskite are 17.85° and 20.76° (**Figure 1f**), respectively, positioning away from iodine atoms. But unlike 2PACZ, 9CPA (18.94°) (**Figure 1g**) and 9CAA (17.09°) (**Figure 1h**) display deviation angles with one iodine in Sn-Pb perovskite, which are close to the iodine atom. The deviation angles identified for 9CAA and 9CPA suggest their more effective coordination with Sn-Pb perovskite to form a more ordered interface, compared with the case of 2PACz. Fourier Transform Infrared Spectrometer (FTIR) spectrum also identified the more effective coordination between 9CAA and Sn-Pb perovskite (Figure S2).

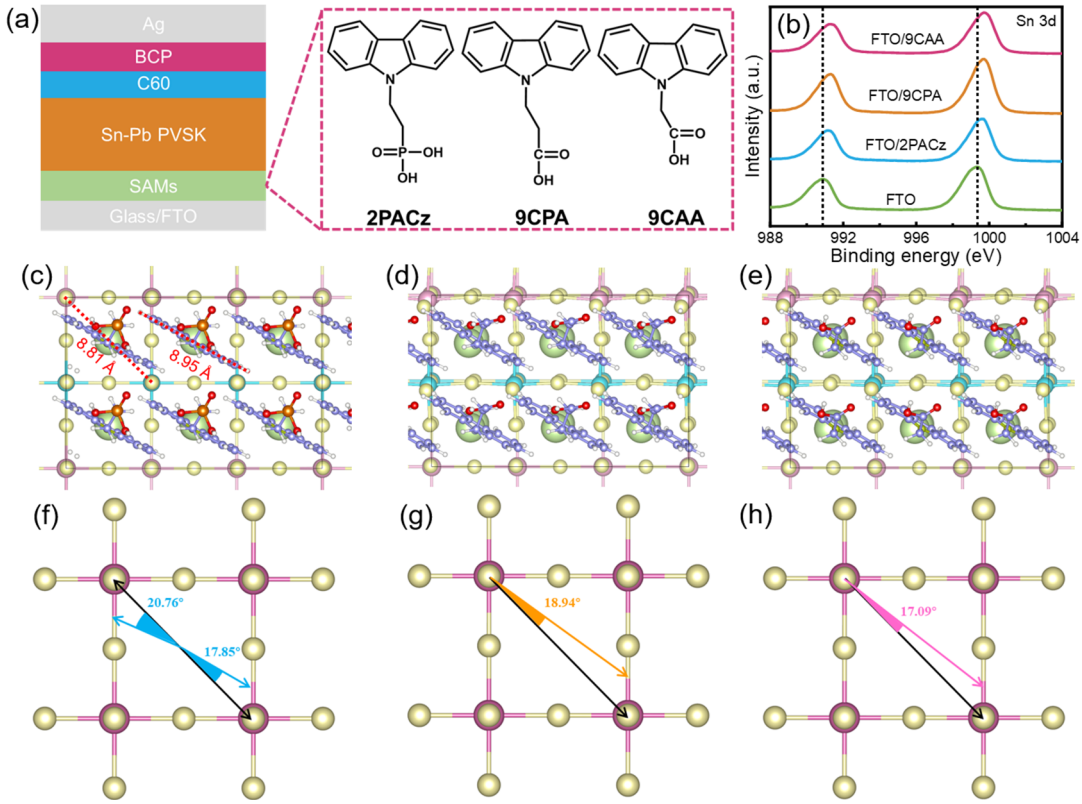

Figure 1. a) The device structure of FTO/SAMs/Sn–Pb perovskite ($Cs_{0.1}FA_{0.6}MA_{0.3}Pb_{0.5}Sn_{0.5}I_3$)/$C_{60}$/BCP/Ag and molecular structure of 2PACz, 9CPA and 9CAA. **b)** XPS spectra of Sn 3d of FTO, FTO/2PACz, FTO/9CPA and FTO/9CAA. The bottom views of **c)** 2PACz/perovskite, **d)** 9CPA/perovskite, and **e)** 9CAA/perovskite structures. The deviation angles of **f)** 2PACz/I atoms, **g)** 9CPA/I atom, and **h)** 9CAA/I atom.

2.2 Energy level alignment

To access the energy levels of FTO/2PACz, FTO/9CPA, FTO/9CAA and Sn–Pb perovskite, we conducted the ultraviolet photoelectron spectroscopy (UPS) measurements (**Figure 2a, b and S3**). As shown in **Figure 2c**, the VBM level of Sn–Pb perovskite is −5.37 eV and the HOMO are −5.35, −5.19 and −4.88 eV for FTO/9CAA, FTO/9CPA and FTO/2PACz, respectively (E_{VB} = 21.22-(E_{Cutoff}-E_i))[41-43]. Comparing VBM and HOMO levels, the FTO/9CAA shows the most favourable energy level alignment for efficient hole extraction from Sn–Pb perovskite [44]. Kelvin probe force microscopy (KPFM) displays the contact potential difference (CPD) values of FTO/2PACz, FTO/9CPA, and FTO/9CAA (**Figure 2d-f**). We obtained the CPD values of −987 (FTO/2PACz, **Figure 2g**), −1073 (FTO/9CPA, **Figure 2h**) and −1164 mV (FTO/9CAA, **Figure 2i**), meaning the work function (WF) of FTO/9CAA is the highest among these three FTO/SAMs, which is beneficial to improved V_{OC}[45]. We also measured transmittance of FTO/SAMs (**Figure S4**) and absorption for FTO/SAMs and FTO/SAMS/Sn–Pb perovskite (**Figure S5 and S6**), which show no optical difference contributed from the SAMs. Therefore, the improved performance may come from favourable energy level alignment.

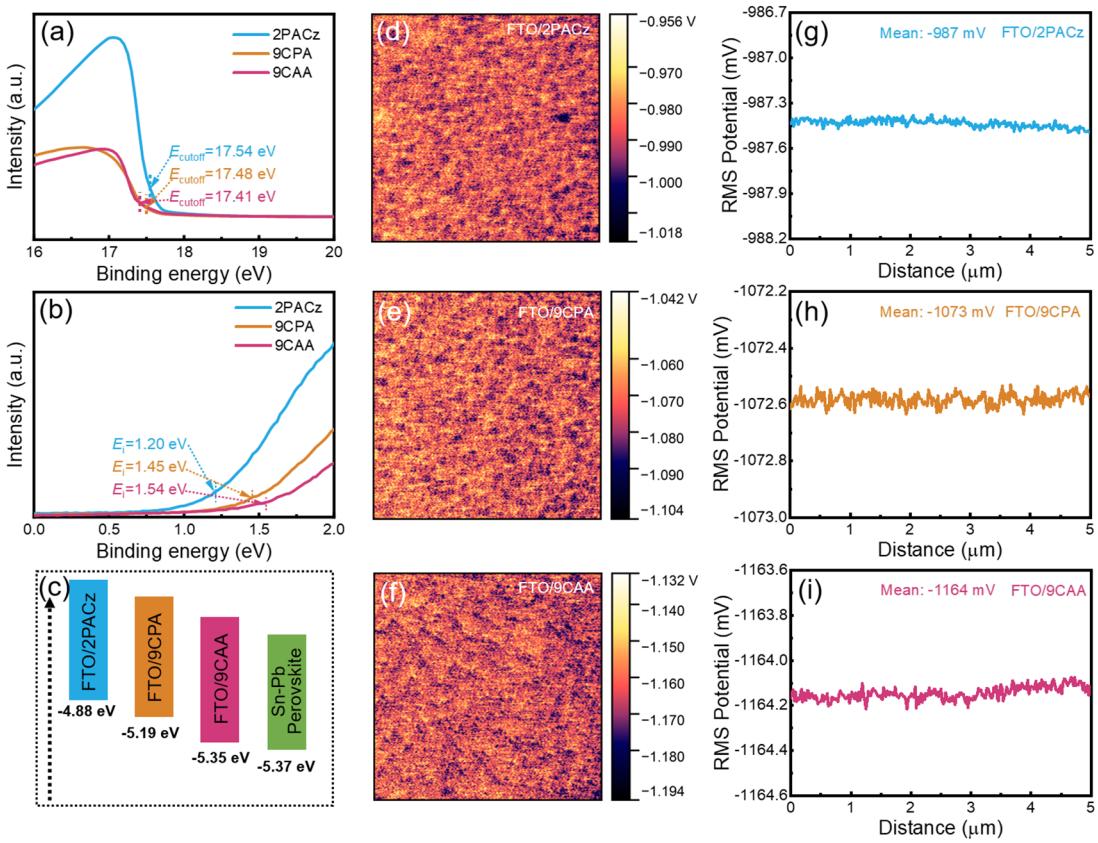

Figure 2. a) E_{cutoff} plots and **b**) E_i plots of FTO/SAMs. **c**) VB alignment of FTO/SAMs and Sn–Pb perovskite. The KPFM images of **d**) FTO/2PACz, **e**) FTO/9CPA and **f**) FTO/CAA. CPD image of **g**) FTO/2PACz, **h**) FTO/9CPA and **i**) FTO/CAA.

2.3 Charge carrier dynamics

Efficient charge carrier extraction is critical for improving the photovoltaic performance of the PSCs. To study charge carrier dynamics in our modified devices, we carried out electrochemical impedance spectroscopy (EIS). As shown in **Figure 3**a, the equivalent circuit for fitting the Nyquist plot displayed recombination resistance (R_{re}) and series resistance (R_s) at low and high frequencies, respectively. The R_{re} of 2PACz-, 9CPA- and 9CAA-based devices are 8163, 11940 and 14731 Ω, respectively. And the R_s are 32, 23 and 21 Ω, respectively. The analysis suggests efficient hole extraction and suppressed interface recombination based on 9CAA-based devices[37, 46]. We plotted photocurrent (J_{ph}) (**Figure S7**) and the charge carriers collection probability ($J_{ph}/J_{ph,\,sat}$, $J_{ph,\,sat}$ represents the saturated photocurrent) (**Figure 3b**) versus the internal voltage (V_{int}) of devices under illumination at AM 1.5G. At the same V_{int}, the 9CAA-based devices showed increased J_{ph} and $J_{ph,\,sat}$, resulting in reduced non-radiative recombination and improved charge carrier collection[47, 48]. We further examined the hole extraction at the buried interface using the transient photocurrent (TPC) measurements. As shown in **Figure 3c**, the 9CAA-based devices display the shortest decay lifetime (0.49 μs) compared with the 9CPA- (0.60 μs) and 2PACz-based devices (0.88 μs) after transmittance excitation of pulse light[49], suggesting a facilitated hole extraction. From these results, we concluded that the 9CAA was the most effective SAM regarding charge carrier management.

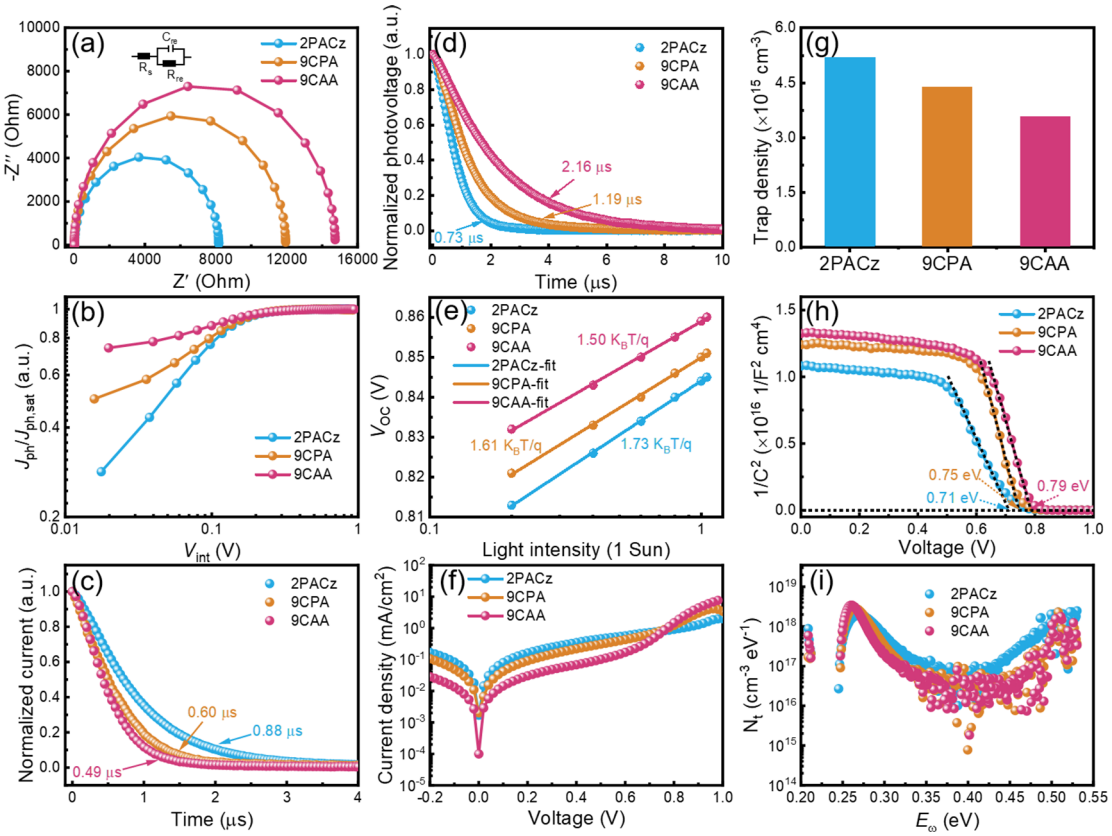

Figure 3. a) EIS **b)** $J_{ph}/J_{ph,\ sat}$ versus V_{int}, **c)** TPC **d)** TPV, and **e)** V_{OC} as a function of light intensity plots of full devices measured in inert atmosphere under AM1.5G illumination. **f)** Dark *J–V* curve of the PSCs. **g)** Trap density histogram extract from SCLC. **h)** Mott−Schottky curve of full devices. **i)** T-DOS plot of full devices.

Recombination occurs at the trap states that are generated by interfacial defects and can also reflect indirectly the interface charge carrier dynamics. As shown in **Figure 3d,** the decay lifetime of transient photovoltage (TPV) of 9CAA-baed device is 2.16 μs, which is substantially longer than that of 9CPA- and 2PACz-based devices at 1.19 and 0.73 μs, respectively. The elongated decay of the 9CAA-based device suggests less amount of charge carriers are captured and recombined at the interface between the 9CAA and the perovskite layer[50, 51]. We also obtained the ideal factor *n* for these structures by the linear fitting of open-circuit voltage (V_{OC}) dependence on light intensity (**Figure 3e**). According to the slopes of linear fitting, the *n* value of 9CAA-, 9CPA- and 2PACz-based devices are 1.50, 1.61 and 1.73, respectively. The smallest *n* value of 9CAA-based devices reveals less Shockley–Read–Hall (SRH) recombination[52]. As shown in **Figure 3f**, the 9CAA-based devices also show the lowest dark current, which again suggests suppressed charge carrier recombination[53, 54].

To analyse the trap density (N_t), we fabricated the hole-only devices based on the structure of FTO/SAMs/perovskite/toluene-based PEDOT/Ag by space-charge-limited current (SCLC) technique (**Figure S8**). According to trap-filed limit voltage (V_{TEL}) values extracted from SCLC curves, the N_t of 9CAA-, 9CPA- and 2PACz-based devices are 3.57×10^{15}, 4.39×10^{15}, and 5.20×10^{15} cm^{-3}, respectively (**Figure 3g**). The reduced N_t profited from improved interfacial contact and lower defect presence. From the Mott−Schottky measurement, the built-in potential (V_{bi}) of devices can be acquired (**Figure 3h**). The value of V_{bi} for 2PACz-based devices is 0.71 V and that of 9CPA- and 9CAA-based devices is increased to 0.75 and 0.79 V, respectively. With the increased V_{bi}, we can expect a stronger force for separating the photogenerated free carriers and driving them to the electrodes[55]. As shown in **Figure 3i**, we also measured the trap density of states (t-DOS) based on the full devices. The 9CAA- and 9CPA-based devices display an order of magnitude lower t-DOS compared to that obtained with the 2PACz-based device,

suggesting fewer defects and non-radiative recombination[56, 57].

2.4 Crystallinity of the perovskite films

To explore the crystallinity of Sn–Pb perovskite, grazing-incidence wide-angle X-ray scattering (GIWAXS) was carried out. As shown in **Figure 4**a-c, the (110) diffraction peak of Sn–Pb perovskite films appears at q_r = 10 nm^{-1} (q = 4πsin(θ)/λ)[58, 59]. According to the XRD diffraction results presented in **Figure 4a-f**, the intensity of (110) reflection of 9CAA-based Sn–Pb perovskite film is considerably stronger than that of 9CPA- and 2PACz-based perovskite films, suggesting the improved crystallinity[37]. This is also further verified with the 1D X-ray diffraction (XRD) measurements (**Figure S9**). We also examined the morphology of the perovskite films using scanning electron microscope (SEM) images. As shown in **Figure 4g-i and S10**, the 9CAA-based Sn–Pb perovskite films display more compact polycrystalline features compared to that of 9CPA- and 2PACz-based films. Meanwhile, the grain sizes of Sn–Pb perovskite films are 625 (9CAA), 611 (9CPA), and 545 nm (2PACz) (**Figure S11**). The 9CAA-based perovskite film also showed the smallest roughness (**Figure S12**). The compact crystal boundaries and enlarged grain sizes in 9CAA-based perovskite films suggest a more favourable interfacial contact, which ultimately leads to devices with improved stability and performance[60-62]. As shown in **Figure S13**, the 9CAA-based perovskite displayed vertical grains, which can reduce non-radiative recombination and enhance charge carrier extraction.

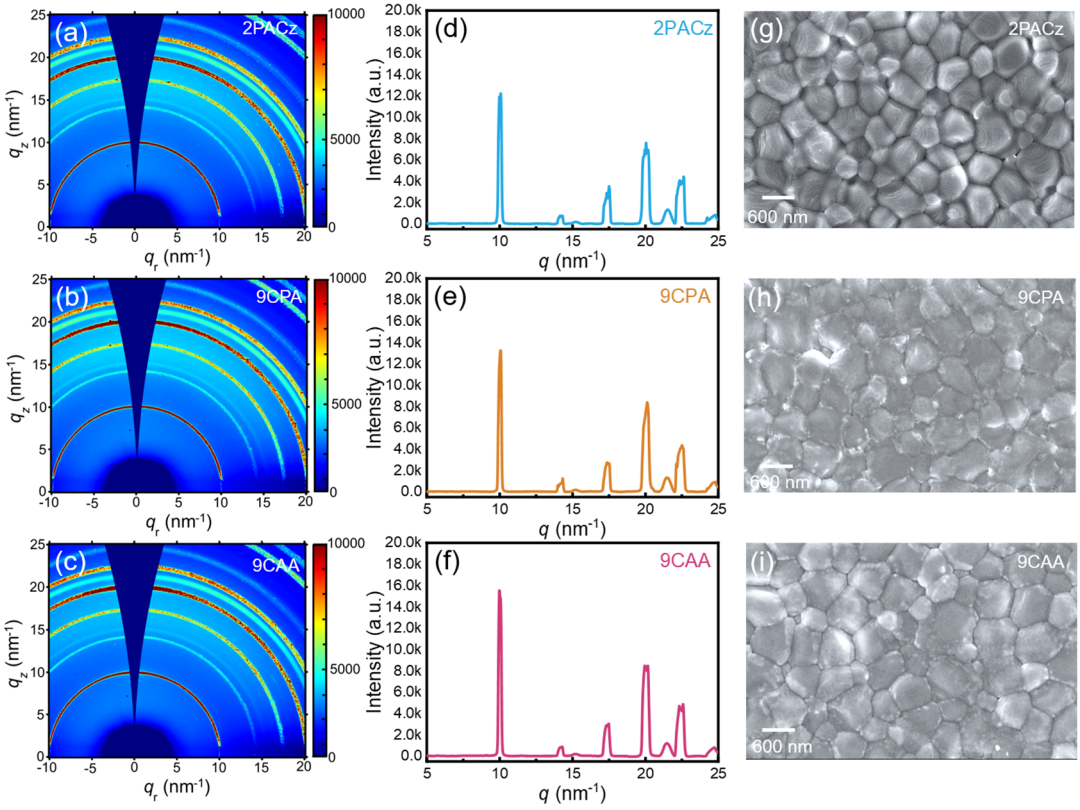

Figure 4. 2D GIWAXS patterns of **a)** 2PACz-, **b)** 9CPA- and **c)** 9CAA-based perovskite films. Azimuthally integrated 1D (out-of-plane direction, azimuth = 90°) of **d)** 2PACz-, **e)** 9CPA-, and **f)** 9CAA-based perovskite films. Top SEM images of **g)** 2PACz-, **h)** 9CPA-, and **i)** 9CAA-based perovskite films.

2.5 Performance of solar cells

To obtain the photovoltaic performance of devices, we applied 2PACz, 9CPA, and 9CAA as the bottom interface modifiers based on the structure of FTO/SAMs/Sn–Pb perovskite/C_{60}/BCP/Ag. To precisely control the concentration of SAM molecules, we set four concentrations 0.1, 0.3, 0.5 and 0.7 mg/mL, and 0.3 mg/mL 9CAA-

based device showed the optimal efficiency (**Figure S14**). In this work, the SAM concentration of SAM molecules is based on 0.3 mg/mL. As shown in **Figure 5**a-c, the 2PACz-based champion device displays a PCE of 20.7% with V_{OC} of 0.86 V, short-circuit current density (J_{SC}) of 32.3 mA/cm^2 and fill factor (FF) of 75%. The 9CPA-based champion device displays a PCE of 22.1% with V_{OC} of 0.89 V, J_{SC} of 32.5 mA/cm^2 and FF of 76%. Finally, the 9CAA-based champion device displays a PCE of 23.1% with V_{OC} of 0.89 V, J_{SC} of 32.8 mA/cm^2 and FF of 79%. The improved photovoltaic performance of 9CAA-based devices is mostly attributed to reduced interface defects and ameliorated interface charge carrier dynamics. The 9CAA-based devices also display neglect hysteresis, which is due to reduced charge accumulation at the interface. The photovoltaic parameters of 30 cells based on different SAMs were analyzed in **Figure S15**, in which 9CAA-based devices show the best photovoltaic performance and reproducibility compared to the 9CPA- and 2PACz-based devices. The incident photon-to-current conversion efficiency (IPCE) was carried out in **Figure 5d**. The integrated J_{SC} are 31.20 (2PACz), 31.63 (9CPA) and 31.99 mA/cm^2 (9CAA), matching with the J_{SC} values measured from J–V characterization. The stabilized output PCE under the maximum power point (MPP) are 22.8%, 21.3% and 19.5% for the 9CAA-, 9CPA- and 2PACz-based devices, respectively (**Figure S16**). We also measured the stability of the devices; the results are provided in **Figure 5e and S17**. The 9CAA-based devices show considerably improved stability with 93% of the initial PCE remaining after 2500 hours of storage in a nitrogen atmosphere, while 9CPA- and 2PACz-based devices retain 89% and 85% of their maximum PCE, respectively, in which the PCE decrease is attributed to FF reduce. And the excellent stability is attributed to favourable interface contact between 9CAA and Sn–Pb perovskite, which can retard the degradation rate[63, 64]. To test the stability of devices in reality conditions, the maximum power point tracking (MPPT) of encapsulated PSCs was carried out under AM 1.5G and ambient. As shown in **Figure S18**, the 9CAA-based device maintained 89% initial PCE, while 9CPA and 2PACz devices maintained 87% and 85% of their initial PCE, which can identify the excellent stability of 9CAA-based devices.

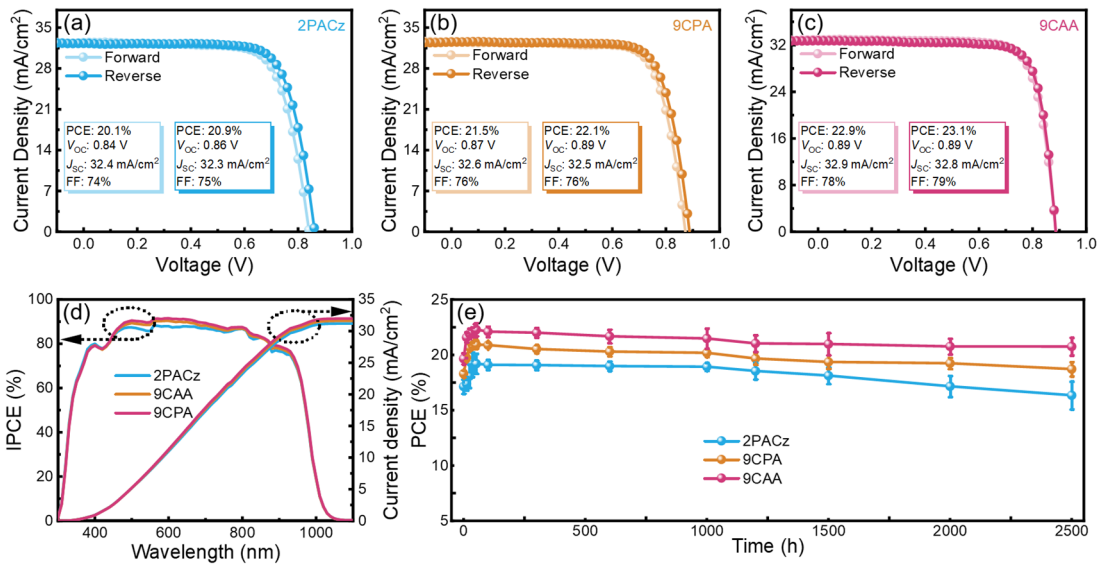

Figure 5. J–V curves of **a**) 2PACz-, **b**) 9CPA- and **c**) 9CAA-based devices. **d**) IPCE curves of full devices. **e**) Stability curves of PCE based on full devices in N_2 atmosphere.

3 Conclusiones

In conclusion, we selected SAMs with diverse functionalisation for improving the characteristics of the buried interface between FTO and Sn–Pb perovskite in the p-i-n devices. The anchoring group and length of the alkyl chain affect the orientation and arrangement of the organic monolayers to different interactions between SAM molecules

and the perovskite layer. The 9CPA and 9CAA display enhanced interaction with Sn–Pb perovskite and conduction substrate than the 2PACz, reducing non-radiative recombination, and improving crystallinity. Besides, we obtained a gradient in VBM alignment in the order of 2PACz > 9CPA > 9CAA > Sn–Pb perovskite, which indicates the most efficient charge carrier extraction from perovskite to the contact in the 9CAA-based devices. Finally, the devices based on 9CAA achieved a PCE of 23.1% and retained 93% of their initial PCE after storage in an inert atmosphere for 2500 hours.

Supporting Information

Supporting Information is available from the Wiley Online Library or the author.

Acknowledgements

Z.Z. and R.Z. contributed equally to this work. The authors thank for the support of the computational resources provided by the Harbin Supercomputer Center. And thanks to beamline BL14B1 and BL03HB at the Shanghai Synchrotron Radiation Facility (SSRF) for providing the beam time. This work was financially supported by the China Postdoctoral Science Foundation (No.2022M721026), the Joint Fund of Provincial Science and Technology Research and Development Plan of Henan Province (No. 232301420004), the National Natural Science Foundation of China (No. 22103022), and Henan Postdoctoral Sustentation (20213036).

Conflict of Interest

The authors declare no conflict of interest.

Data Availability Statement

Research data are not shared.

[1] NREL, Best Research-Cell Efficiency Chart, https://www.nrel.gov/pv/assets/pdfs/best-research-cell-efficiencies.pdf, November 2023

[2] M. M. Lee, J. Teuscher, T. Miyasaka, T. N. Murakami, H. J. Snaith, *science* **2012**, *338*, 643.

[3] A. Kojima, K. Teshima, Y. Shirai, T. Miyasaka, *J. Am. Chem. Soc.* **2009**, *131*, 6050.

[4] S. D. Stranks, H. J. Snaith, *Nat. Nanotechnol.* **2015**, *10*, 391.

[5] M. Liu, M. B. Johnston, H. J. Snaith, *Nature* **2013**, *501*, 395.

[6] O. Malinkiewicz, A. Yella, Y. H. Lee, G. M. Espallargas, M. Graetzel, M. K. Nazeeruddin, H. J. Bolink, *Nat. Photonics* **2014**, *8*, 128.

[7] J. Park, J. Kim, H.-S. Yun, M. J. Paik, E. Noh, H. J. Mun, M. G. Kim, T. J. Shin, S. I. Seok, *Nature* **2023**, *616*, 724.

[8] Q. Tan, Z. Li, G. Luo, X. Zhang, B. Che, G. Chen, H. Gao, D. He, G. Ma, J. Wang, J. Xiu, H. Yi, T. Chen, Z. He, *Nature* **2023**, *620*, 545.

[9] W. Shockley, H. J. Queisser, *J. Appl. Phys.* **1961**, *32*, 510.

[10] S. Hu, K. Otsuka, R. Murdey, T. Nakamura, M. A. Truong, T. Yamada, T. Handa, K. Matsuda, K. Nakano, A. Sato, K. Marumoto, K. Tajima, Y. Kanemitsu, A. Wakamiya, *Energy Environ. Sci.* **2022**, *15*, 2096.

[11] R. Lin, Y. Wang, Q. Lu, B. Tang, J. Li, H. Gao, Y. Gao, H. Li, C. Ding, J. Wen, P. Wu, C. Liu, S. Zhao, K. Xiao, Z. Liu, C. Ma, Y. Deng, L. Li, F. Fan, H. Tan, *Nature* **2023**, *620*, 994.

[12] G. Kapil, T. Bessho, Y. Sanehira, S. R. Sahamir, M. Chen, A. K. Baranwal, D. Liu, Y. Sono, D. Hirotani, D. Nomura, K. Nishimura, M. A. Kamarudin, Q. Shen, H. Segawa, S. Hayase, *ACS Energy Lett.* **2022**, *7*, 966.

[13] Z. Yu, J. Wang, B. Chen, M. A. Uddin, Z. Ni, G. Yang, J. Huang, *Adv. Mater.* **2022**, *34*, 2205769.

[14] F. Hao, C. C. Stoumpos, R. P. Chang, M. G. Kanatzidis, *J. Am. Chem. Soc.* **2014**, *136*, 8094.

[15] A. Goyal, S. McKechnie, D. Pashov, W. Tumas, M. Van Schilfgaarde, V. Stevanovic, *Chem. Mater.* **2018**, *30*, 3920.

[16] G. E. Eperon, T. Leijtens, K. A. Bush, R. Prasanna, T. Green, J. T.-W. Wang, D. P. McMeekin, G. Volonakis, R. L. Milot, R. May, A. Palmstrom, D. J. Slotcavage, R. A. Belisle, J. B. Patel, E. S. Parrott, R. J. Sutton, W. Ma, F. Moghadam, B. Conings, A. Babayigit, H.-G. Boyen, S. Bent, F. Giustino, L. M. Herz, M. B. Johnston, M. D. McGehee, H. J. Snaith, *Science* **2016**, *354*, 861.

[17] D. P. McMeekin, S. Mahesh, N. K. Noel, M. T. Klug, J. Lim, J. H. Warby, J. M. Ball, L. M. Herz, M. B. Johnston, H. J. Snaith, *Joule* **2019**, *3*, 387.

[18] J. Wang, V. Zardetto, K. Datta, D. Zhang, M. M. Wienk, R. A. Janssen, *Nat. Commun.* **2020**, *11*, 5254.

[19] M. T. Hörantner, T. Leijtens, M. E. Ziffer, G. E. Eperon, M. G. Christoforo, M. D. McGehee, H. J. Snaith, *ACS Energy Lett.* **2017**, *2*, 2506.

[20] R. He, W. Wang, Z. Yi, F. Lang, C. Chen, J. Luo, J. Zhu, J. Thiesbrummel, S. Shah, K. Wei, Y. Luo, C. Wang, H. Lai, H. Huang, J. Zhou, B. Zou, X. Yin, S. Ren, X. Hao, L. Wu, J. Zhang, J. Zhang, M. Stolterfoht, F. Fu, W. Tang, D. Zhao, *Nature* **2023**, *618*, 80.

[21] M. A. Green, E. D. Dunlop, M. Yoshita, N. Kopidakis, K. Bothe, G. Siefer, X. Hao, *Prog Photovolt Res Appl.* **2023**, *31*, 651.

[22] A. Al-Ashouri, E. Köhnen, B. Li, A. Magomedov, H. Hempel, P. Caprioglio, J. A. Márquez, A. B. Morales Vilches, E. Kasparavicius, J. A. Smith, N. Phung, D. Menzel, M. Grischek, L. Kegelmann, D. Skroblin, C. Gollwitzer, T. Malinauskas, M. Jošt, G. Matičˇ, B. Rech, R. Schlatmann, M. Topičˇ, L. Korte, A. Abate, B. Stannowski, D. Neher, M. Stolterfoht, T. Unold, V. Getautis, S. Albrecht, *Science* **2020**, *370*, 1300.

[23] G. Li, Z. Su, L. Canil, D. Hughes, M. H. Aldamasy, J. Dagar, S. Trofimov, L. Wang, W. Zuo, J. J. Jerónimo-Rendon, M. M. Byranvand, C. Wang, R. Zhu, Z. Zhang, F. Yang, G. Nasti, B. Naydenov, W. C. Tsoi, Z. Li, X. Gao, Z. Wang, Y. Jia, E. Unger, M. Saliba, M. Li, A. Abate, *Science* **2023**, *379*, 399.

[24] H. L. Yip, S. K. Hau, N. S. Baek, H. Ma, A. K. Y. Jen, *Adv. Mater.* **2008**, *20*, 2376.

[25] I. Lange, S. Reiter, M. Pätzel, A. Zykov, A. Nefedov, J. Hildebrandt, S. Hecht, S. Kowarik, C. Wöll, G. Heimel, D. Neher, *Adv. Funct. Mater.* **2014**, *24*, 7014.

[26] W. Jiang, F. Li, M. Li, F. Qi, F. R. Lin, A. K. Y. Jen, *Angew. Chem. Int. Ed.* **2022**, *61*, e202213560.

[27] Y. Yao, C. Cheng, C. Zhang, H. Hu, K. Wang, S. De Wolf, *Adv. Mater.* **2022**, *34*, 2203794.

[28] A. Al-Ashouri, A. Magomedov, M. Roß, M. Jošt, M. Talaikis, G. Chistiakova, T. Bertram, J. A. Márquez, E. Köhnen, E. Kasparavičius, S. Levcenco, L. Gil-Escrig, C. J. Hages, R. Schlatmann, B. Rech, T. Malinauskas, T. Unold, C. A. Kaufmann, L. Korte, G. Niaura, V. Getautis, S. Albrecht, *Energy Environ. Sci.* **2019**, *12*, 3356.

[29] M. A. Truong, T. Funasaki, L. Ueberricke, W. Nojo, R. Murdey, T. Yamada, S. Hu, A. Akatsuka, N. Sekiguchi, S. Hira, L. Xie, T. Nakamura, N. Shioya, D. Kan, Y. Tsuji, S. Iikubo, H. Yoshida, Y. Shimakawa, T. Hasegawa, Y. Kanemitsu, T. Suzuki, A. Wakamiya, *J. Am. Chem. Soc.* **2023**, *145*, 7528.

[30] J. Y. Seo, S. Akin, M. Zalibera, M. A. R. Preciado, H. S. Kim, S. M. Zakeeruddin, J. V. Milić, M. Grätzel, *Adv. Funct. Mater.* **2021**, *31*, 2102124.

[31] L. Xu, X. Chen, J. Jin, W. Liu, B. Dong, X. Bai, H. Song, P. Reiss, *Nano Energy* **2019**, *63*, 103860.

[32] I. Levine, A. Al-Ashouri, A. Musiienko, H. Hempel, A. Magomedov, A. Drevilkauskaite, V. Getautis, D. Menzel, K. Hinrichs, T. Unold, S. Albrecht, T. Dittrich, *Joule* **2021**, *5*, 2915.

[33] Y. Lin, Y. Firdaus, F. H. Isikgor, M. I. Nugraha, E. Yengel, G. T. Harrison, R. Hallani, A. El-Labban, H. Faber, C. Ma, X. Zheng, A. Subbiah, C. T. Howells, O. M. Bakr, I. McCulloch, S. D. Wolf, L. Tsetseris, T. D. Anthopoulos, *ACS Energy Lett.* **2020**, *5*, 2935.

[34] S. M. Park, M. Wei, N. Lempesis, W. Yu, T. Hossain, L. Agosta, V. Carnevali, H. R. Atapattu, P. Serles, F. T. Eickemeyer, H. Shin, M. Vafaie, D. Choi, K. Darabi, E. D. Jung, Y. Yang, D. B. Kim, S. M. Zakeeruddin, B. Chen, A. Amassian, T. Filleter, M. G. Kanatzidis, K. R. Graham, L. Xiao, U. Rothlisberger, M. Grätzel, E. H. Sargent, *Nature* **2023**, 1.

[35] Z. Chen, Y. Li, Z. Liu, J. Shi, B. Yu, S. Tan, Y. Cui, C. Tan, F. Tian, H. Wu, Y. Luo, D. Li, Q. Meng, *Adv. Energy Mater.* **2023**, *13*, 2202799.

[36] Y. Dong, W. Shen, W. Dong, C. Bai, J. Zhao, Y. Zhou, F. Huang, Y. B. Cheng, J. Zhong, *Adv. Energy Mater.* **2022**, *12*, 2200417.

[37] C. Xu, S. Zhang, W. Fan, F. Cheng, H. Sun, Z. Kang, Y. Zhang, *Adv. Mater.* **2023**, *35*, 2207172.

[38] X. Zuo, B. Kim, B. Liu, D. He, L. Bai, W. Wang, C. Xu, Q. Song, C. Jia, Z. Zang, D. Lee, X. Li, J. Chen, *Chem. Eng. J* **2022**, *431*, 133209.

[39] C. Luo, G. Zheng, F. Gao, X. Wang, C. Zhan, X. Gao, Q. Zhao, *Nat. Photonics* **2023**, *17*, 856.

[40] H. Xu, Y. Miao, N. Wei, H. Chen, Z. Qin, X. Liu, X. Wang, Y. Qi, T. Zhang, Y. Zhao, *Adv. Energy Mater.* **2022**, *12*, 2103151.

[41] J. A. Hong, M. Jeong, S. Park, A. Y. Lee, H. S. Kim, S. Jeong, D. W. Kim, S. Cho, C. Yang, M. H. Song, *Adv. Sci.* **2023**, *10*, 2205127.

[42] L. Wang, M. Chen, S. Yang, N. Uezono, Q. Miao, G. Kapil, A. K. Baranwal, Y. Sanehira, D. Wang, D. Liu, T. Ma, K. Ozawa, T. Sakurai, Z. Zhang, Q. Shen, S. Hayase, *ACS Energy Lett.* **2022**, *7*, 3703.

[43] M. Hu, A. M. Risqi, J. Wu, L. Chen, J. Park, S. U. Lee, H. S. Yun, B. W. Park, C. J. Brabec, S. I. Seok, *Adv. Funct. Mater.* **2023**, 2300693.

[44] S. Hu, P. Zhao, K. Nakano, R. D. Oliver, J. Pascual, J. A. Smith, T. Yamada, M. A. Truong, R. Murdey, N. Shioya, T. Hasegawa, M. Ehara, M. B. Johnston, K. Tajima, Y. Kanemitsu, H. J. Snaith, A. Wakamiya, *Adv. Mater.* **2023**, *35*, 2208320.

[45] D. Yang, R. Yang, K. Wang, C. Wu, X. Zhu, J. Feng, X. Ren, G. Fang, S. Priya, S. Liu, *Nat. Commun.* **2018**, *9*, 3239.

[46] X. Jiang, C. Li, X. Wang, C. Peng, H. Jiang, H. Bu, M. Zhu, H. Yin, B. He, H. Li, S. Pang, Z. Zhou, *ACS Energy Lett.* **2023**, *8*, 1068.

[47] A. K. K. Kyaw, D. H. Wang, D. Wynands, J. Zhang, T.-Q. Nguyen, G. C. Bazan, A. J. Heeger, *Nano Lett.* **2013**, *13*, 3796.

[48] Z. Xing, M.-W. An, Z.-C. Chen, M. Hu, X. Huang, L.-L. Deng, Q. Zhang, X. Guo, S.-Y. Xie, S. Yang, *J. Am. Chem. Soc.* **2022**, *144*, 13839.

[49] L. Meng, C. Sun, R. Wang, W. Huang, Z. Zhao, P. Sun, T. Huang, J. Xue, J.-W. Lee, C. Zhu, Y. Huang, Y. Li, Y. Yang, *J. Am. Chem. Soc.* **2018**, *140*, 17255.

[50] J. Wu, M.-H. Li, J.-T. Fan, Z. Li, X.-H. Fan, D.-J. Xue, J.-S. Hu, *J. Am. Chem. Soc.* **2023**, *145*, 5872.

[51] B. Li, J. Deng, J. A. Smith, P. Caprioglio, K. Ji, D. Luo, J. D. McGettrick, K. I. Jayawardena, R. C. Kilbride, A. Ren, S. Hinder, J. Bi, T. Webb, I. Marko, X. Liu, Y. Xiang, J. Reding, H. Li, S. Du, D. G. Lidzey, S. D. Stranks, T. Watson, S. Sweeney, H. J. Snaith, S. R. P. Silva, W. Zhang, *Adv. Energy Mater.* **2022**, *12*, 2202868.

[52] J. Zhang, Y. Sun, C. Huang, B. Yu, H. Yu, *Adv. Energy Mater.* **2022**, *12*, 2202542.

[53] C. Li, Z. Song, D. Zhao, C. Xiao, B. Subedi, N. Shrestha, M. M. Junda, C. Wang, C. S. Jiang, M. Al-Jassim, R. J. Ellingson, N. J. Podraza, K. Zhu, Y. Yan, *Adv. Energy Mater.* **2019**, *9*, 1803135.

[54] T. Wang, Y. Li, Q. Cao, J. Yang, B. Yang, X. Pu, Y. Zhang, J. Zhao, Y. Zhang, H. Chen, A. Hagfeldt, X. Li, *Energy Environ. Sci.* **2022**, *15*, 4414.

[55] X. Li, W. Zhang, X. Guo, C. Lu, J. Wei, J. Fang, *Science* **2022**, *375*, 434.

[56] C. Liu, Y. Yang, O. A. Syzgantseva, Y. Ding, M. A. Syzgantseva, X. Zhang, A. M. Asiri, S. Dai, M. K.

Nazeeruddin, *Adv. Mater.* **2020**, *32*, 2002632.

[57] R. Azmi, N. Nurrosyid, S.-H. Lee, M. Al Mubarok, W. Lee, S. Hwang, W. Yin, T. K. Ahn, T.-W. Kim, D. Y. Ryu, Y. R. Do, S.-Y. Jang, *ACS Energy Lett.* **2020**, *5*, 1396.

[58] G. Li, Z. Su, M. Li, F. Yang, M. H. Aldamasy, J. Pascual, F. Yang, H. Liu, W. Zuo, D. Di Girolamo, Z. Iqbal, G. Nasti, A. Dallmann, X. Gao, Z. Wang, M. Saliba, A. Abate, *Adv. Energy Mater.* **2021**, *11*, 2101539.

[59] H. Liu, Z. Zhang, Z. Su, W. Zuo, Y. Tang, F. Yang, X. Zhang, C. Qin, J. Yang, Z. Li, M. Li, *Adv. Sci.* **2022**, *9*, 2105739.

[60] R. Chen, J. Wang, Z. Liu, F. Ren, S. Liu, J. Zhou, H. Wang, X. Meng, Z. Zhang, X. Guan, W. Liang, P. A. Troshin, Y. Qi, L. Han, W. Chen, *Nat. Energy* **2023**, *8*, 839.

[61] C. Ding, L. Yin, J. Wang, V. Larini, L. Zhang, R. Huang, M. Nyman, L. Zhao, C. Zhao, W. Li, Q. Luo, Y. Shen, R. Österbacka, G. Grancini, C.-Q. Ma, *Adv. Mater.* **2023**, *35*, 2207656.

[62] Q. Hu, W. Chen, W. Yang, Y. Li, Y. Zhou, B. W. Larson, J. C. Johnson, Y.-H. Lu, W. Zhong, J. Xu, L. Klivansky, C. Wang, M. Salmeron, A. B. Djurišić, F. Liu, Z. He, R. Zhu, T. P. Russell, *Joule* **2020**, *4*, 1575.

[63] F. Ye, S. Zhang, J. Warby, J. Wu, E. Gutierrez-Partida, F. Lang, S. Shah, E. Saglamkaya, B. Sun, F. Zu, S. Shoaee, H. Wang, B. Stiller, D. Neher, W.-H. Zhu, M. Stolterfoht, Y. Wu, *Nat. Commun.* **2022**, *13*, 7454.

[64] J. Zhu, Y. Luo, R. He, C. Chen, Y. Wang, J. Luo, Z. Yi, J. Thiesbrummel, C. Wang, F. Lang, H. Lai, Y. Xu, J. Wang, Z. Zhang, W. Liang, G. Cui, S. Ren, X. Hao, H. Huang, Y. Wang, F. Yao, Q. Lin, L. Wu, J. Zhang, M. Stolterfoht, F. Fu, D. Zhao, *Nat. Energy* **2023**, 1.